JOURNAL OF PROPULSION AND POWER
Vol. 11, No. 1, January–February 1995

Velocity Measurements Downstream of a Lobed-Forced Mixer with Different Trailing-Edge Configurations

Simon C. M. Yu,* Joon H. Yeo,† and Jeffrey K. L. Teh‡
Nanyang Technological University, 2263 Singapore

Velocity and turbulence characteristics have been measured downstream of a lobed-forced mixer with three different trailing-edge configurations, using a two-component laser-Doppler anemometer at a Reynolds number of 2.27 × 10⁴ (based on the bulk mean velocity of the two streams at 10 m/s, and a nominal wavelength of the lobe at 33 mm), and with velocity ratios of 1:1, 1:2, and 1:3 across the lobe. The three trailing-edge configurations under investigation have the shape of a square wave, a semicircular wave, and a triangular wave. The results for the velocity ratio 1:1 indicate that the mixing is not only affected by the strength of the secondary flow shed by a lobe, but also by the boundary-layer thickness grown along the sidewalls of the lobe penetration and the subsequent shedding of the boundary layer to the wake region. No region of high turbulence was found within six wavelengths downstream of the trailing edge. The results for the higher velocity ratios, 1:2 and 1:3, reveal a very different flow development from those of an equal velocity ratio. A high-turbulence region appeared at around two to three wavelengths downstream of the trailing edge, and was followed by a gradual decay in magnitude. Analyzing the production terms in the Reynolds stresses equations at the corresponding location suggested that positive production of turbulent kinetic energy existed and was a consequence of large mean axial velocity gradients that coincided with shear stresses of the opposite signs. Thus, the present investigations suggest that the high-turbulence region responsible for rapid mixing may not be due to vortex breakdown (at six wavelengths downstream), but may be due to the positive production of turbulent kinetic energy at a location (at about two to three wavelengths downstream) earlier than previously suggested.

Nomenclature

A_{wake}	=	cross-sectional area bounded by the wake region
C_1	=	normalized streamwise circulation, $\Gamma_s/U_r h \tan \varepsilon$
H	=	boundary-layer shape factor, δ^*/Θ
h	=	lobe height, 33 mm
k	=	turbulent kinetic energy, $\frac{1}{2}(u'^2 + v'^2 + w'^2)$
Re	=	Reynolds number, $U_r\lambda/\nu$, 2.27 × 10⁴
Re_Θ	=	Reynolds number based on the momentum thickness
S	=	shape factor, $(\int U^2\, dA_{wake}/U_r^2 A_{wake})$
U, u'	=	streamwise mean and the corresponding rms velocities
U_r	=	reference mean velocity, $(U_1 + U_2)/2$, 10 m/s
U_s	=	secondary mean velocity, $\sqrt{v^2 + w^2}$
U_1, U_2	=	mean velocity of the top and bottom streams
$\overline{u'v'}, \overline{u'w'}$	=	Reynolds shear stresses
V, v'	=	horizontal mean and the corresponding rms velocities
W, w'	=	vertical mean and the corresponding rms velocities
x, y, z	=	streamwise, horizontal, and vertical directions
Γ_s	=	streamwise circulation
δ^*	=	displacement thickness, mm
ε	=	half of the included divergent angle of the penetration region, 22 deg
Θ	=	momentum thickness, mm
λ (or $2 \times B$)	=	nominal lobe wavelength, 33 mm
ν	=	kinematic viscosity

Received Nov. 4, 1993; presented as Paper 94-0018 at the AIAA 32nd Aerospace Sciences Meeting and Exhibit, Reno, NV, Jan. 10–13, 1994; revision received May 2, 1994; accepted for publication May 5, 1994.

*Lecturer, Thermal Engineering Division, School of Mechanical and Production Engineering. Member AIAA.
†Lecturer, Thermal Engineering Division, School of Mechanical and Production Engineering.
‡Research Assistant, Thermal Engineering Division, School of Mechanical and Production Engineering. Member AIAA.

Introduction

SPLITTER plates with a convoluted trailing edge (commonly referred to as lobed-forced mixers) are passive, fluid mechanical devices that generate in the coflowing streams a three-dimensional shear layer with strong secondary flow. As shown in Fig. 1, the geometry of a lobed-forced mixer is characterized by a periodically alternating, lobed trailing-edge surface. The lobe causes large-scale streamwise vortices to be shed at the trailing edge so that the downstream flowfield is embedded with an array of streamwise vortices of alternating sign. The enhanced mixing of the lobed mixers is believed to be directly attributable to the large mixing scales generated by the streamwise vortices. Application of lobed mixers in the turbofan engine exhausts have been previously studied,[1–3] where the rapid mixing of the core and the bypass flows can achieve noise reduction and thrust enhancement. However, in those investigations, only the gross features of the flowfield were investigated.

Paterson[4,5] measured velocity and turbulence characteristics downstream of a lobed mixer using laser-Doppler anemometer, and concluded that both the lobe shape and penetration were the important parameters in determining the effectiveness of mixer performances. Paterson also found that

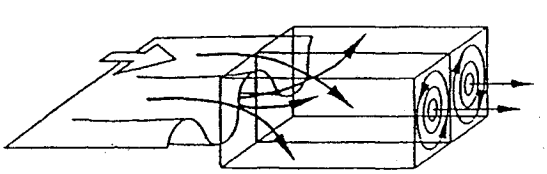

Fig. 1 Wake flow structure behind the convoluted trailing edge.[7]

the generation of streamwise vortices was due mainly to the secondary flow shed by the lobe and, therefore, concluded that the streamwise vortices were inviscidly generated. The subsequent investigation by Barber et al.[6] confirmed the inviscid nature of the secondary flow generated by a lobe, and the strength of the secondary flow was also found to be higher when the lobe penetration consisted of straight parallel sidewalls. They also found that higher strength would result in a faster mixing rate and, hence, would facilitate the condition of achieving spatial uniformity downstream of the mixer. However, in their investigation, measurements were obtained at only one location, about one-half wavelength downstream of the mixers, and no direct comparisons of the flow structures were performed between different configurations at the downstream locations.

Based on flow visualization tests in a water tunnel, Werle et al.[7] suggested that the flow structure of the wake region behind the lobed mixer follow a three-step process by which the streamwise vortex cells form, intensify, and then break down. Most intense mixing seemed to occur in the third region. The laser-Doppler velocity measurements (at velocity ratios of 1:1 and 1:2; $h/B = 2$ and $\varepsilon = 13.5$ deg) of Eckerle et al.[8] appeared to support this observation. Their analysis was based on a spatial averaging of the measured normal and shear stress components on the transverse planes at downstream locations within six wavelengths of the mixer trailing edge. By varying the velocity ratio across the lobe, the location of these three regions could be shifted.

Water-tunnel visualization tests by Manning[9] had shown that both the streamwise vorticity and the accompanying increase in initial interfacial area (due to the convoluted trailing edge comparing to a flat plate) were significant contributors to the mixing enhancement of forced lobed mixers. The enhancement of mixing was also found to be stronger as the velocity ratio across the lobe increased.

Recent velocity measurements (at a velocity ratio 1:2; $h/B = 3$ and $\varepsilon = 15$ deg) by McCormick and Bennett,[10] using the triple-sensor hot film probe, in a lobed mixer similar to that of Eckerle et al., concluded that the intense small-scale turbulence and mixing that occurred at about two to four wavelengths downstream of the mixer trailing edge is due mainly to the deformation of the normal vortex into a pinched-off structure by the streamwise vorticity. In the present investigation, it will be shown that no region of high turbulence was found within six wavelengths downstream of the mixer trailing edge for the velocity ratio of 1:1, and for the cases of 1:2 and 1:3 it appeared at around two to three wavelengths downstream of the mixer.

The main objective of the present investigation is to present the detailed results of a comparative study of the flow structures obtained with mixers of different trailing-edge configurations, but with equal penetration angle, wavelength, and the same upstream conditions. It is also the continuation of a preliminary investigation on the flow structure behind the lobed mixers at velocity ratio of 1:1 across the lobe as described briefly in Ref. 11. Three trailing-edge configurations of the lobed-forced mixer have been investigated using a laser-Doppler anemometer at velocity ratios of 1:1, 1:2, and 1:3 across the lobe: a square wave, a semicircular wave, and the triangular (saw-tooth) wave. The data obtained may also be used for validation of different CFD methods and turbulence models.

While actual velocity measurements can provide a detailed picture of the wake region, flow visualization studies were also conducted in the present investigation to provide a qualitative understanding of the wake region. The smoke-wire and laser-sheet visualization techniques have been used.

The following section briefly describes the experimental setups for both flow visualization and velocity measurement purposes, including the laser-Doppler anemometer. It will be followed by a presentation and discussion of the results. This article ends with a summary of important findings.

Flow Configurations and Instrumentation

Flow Visualization

Flow visualization experiments were performed in a low-speed, low-turbulence, open-circuit suction-type wind tunnel, designed especially for smoke-wire visualization applications. The test section was 100 mm high, 200 mm wide, and 700 mm long. The bulk mean velocity could be varied from 1 to 2.5 m/s. The streamwise turbulence level for this velocity range within the test section was less than 0.5% of the bulk velocity measured by a constant temperature anemometer. The experiments were carried out at a mean flow velocity of 2 m/s and at a velocity ratio of 1:1 across the lobe, which corresponded to a Reynolds number of 4.54×10^3 (based on the nominal wavelength of the lobe at 33 mm). Such flow velocity had been chosen, after some preliminary experiments, in order to obtain the best recordable pictures.

The smoke-wire visualization method used in the experiment consisted of thin wires with 180 mm length and 100-W/m specific resistance. The wire was heated at a voltage of 20–30 V during the course of the experiment. The heating time was adjusted within 100–400 ms. Positions of the wires are indicated in Fig. 3. The smoke was illuminated by two methods: 1) a flash (for photographs shown in Fig. 3), and 2) a light sheet from a 1-W argon laser combined with a cylindrical lens (for photographs shown in Fig. 4).

Wind Tunnel

The wind tunnel used for velocity measurements in the present investigation was an open-circuit, suction-type, which has a contraction of area ratio 10:1 (see Fig. 2a). This large contraction ratio ensured an uniform core flow and a relative low turbulence level (<1% of the inlet bulk velocity) at entry to the test section. The Plexiglas® test section is 200 mm high, 200 mm wide, and 500 mm long. The model lobed mixer was mounted at the entrance to the test section in a central position so that on each side of the splitter plate there was the same area of flow. Different velocity ratios between the upper and lower streams were achieved by incorporating screens and wire meshes on one side of the lobed mixer. The speed range of the wind tunnel in the absence of the lobed mixer was from 1 to 25 m/s. In the present investigation, a mean speed of 10 m/s had been used, corresponding to a Reynolds number of 2.27×10^4 (based on the nominal wavelength of the lobe at 33 mm).

Lobed Mixer Configurations

The lobed mixers were made of 2-mm-thick fiberglass with a round leading edge facing the entrance of the test section. Each mixer has six full lobes with a nominal wavelength of 33 mm. The lobe penetration region is about 11% of the total length of the mixer (360 mm) with an included divergence angle of 44 deg. The coordinate system adopted in the present experiment is shown in Fig. 2b.

Measurements of the three-orthogonal mean velocities (U, V, W), their corresponding rms fluctuations (u', v', w'), and Reynolds shear stresses ($\overline{u'v'}$, $\overline{u'w'}$) were acquired in the projected area corresponding to the one lobe located close to the center of the test section, i.e., at the third lobe from the sidewall of the test section, and at downstream locations where $x/\lambda = 0.5$, 2, 4, and 6 (also see Fig. 2a). At each station, there were about 81 measuring points. The turbulent boundary-layer thickness of the velocity profiles, on either side of the lobed mixer and at three wavelengths upstream of the penetration region for different velocity ratios were measured by a pitot static tube with a nominal diameter of 1 mm. The pitot static tube output was connected to a differential micromanometer with accuracy of 0.01-mm water level.

Laser-Doppler Anemometer

Three orthogonal velocities, their corresponding rms fluctuations and Reynolds shear stresses, were measured using a three-beam, two-component laser-Doppler anemometer

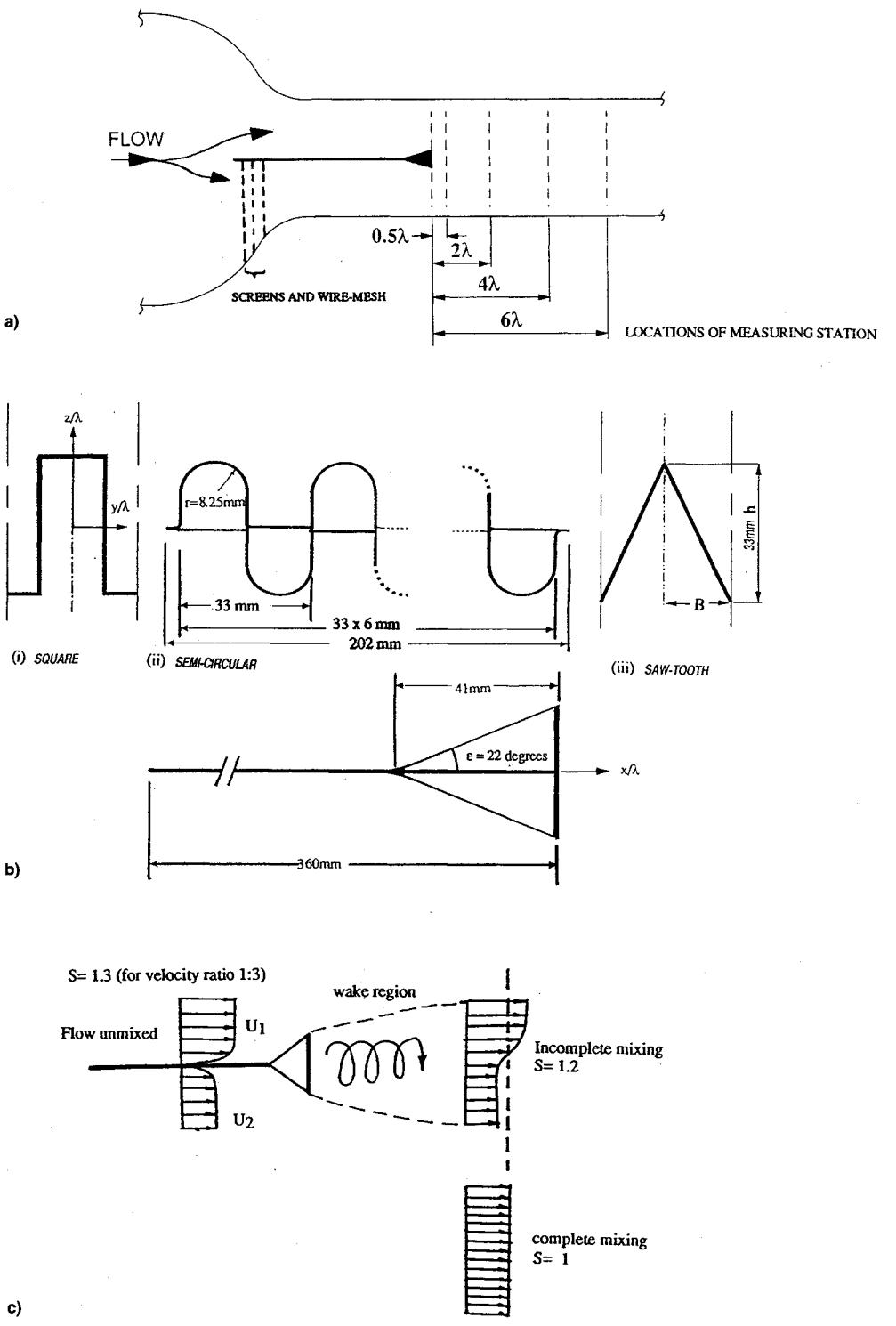

Fig. 2 a) Schematic of the test section, b) lobed mixer configurations under investigation, and c) definition of shape factor for various degrees of mixing.

(Dantec 55X series) with a 3-W Argon laser operating in a backscattered mode. A focusing lens of 310 mm provided an (average) measuring probe volume of 0.01 × 0.01 × 1.1 mm. An automated two-dimensional traversing system was used, with an accuracy of ±0.001 mm. Bragg shifting of frequency up to 2 MHz was used for directional ambiguity. The Doppler signals were detected by photomultipliers and processed by counter-type signal processors. Fine water droplets, sizes ranging from 2 to 5 μm generated by a commercially available atomizer (Dantec 55L18) were used to seed the flow. At each measuring point, the mean velocities, the rms of the velocity fluctuations, and the Reynolds shear stresses were determined from populations of more than 2000 (on each channel) samples together with a coincidence window of 30 μs. Other coincidence window widths from 30 to 100 μs were also tested, but no significant difference in the results were found. Each individual measurement was required to satisfy the counter "5/8" validation comparison within a preset tolerance of 3%. Measurements were repeated twice to ensure reproducibility. The accuracy of the measured velocity components (normalized by the bulk mean velocity of the two streams U_r, 10 m/s) was always better than 2%, and that of the rms of the velocity fluctuations (normalized by U_r) and the Reynolds shear stresses (normalized by U_r^2), 5%.

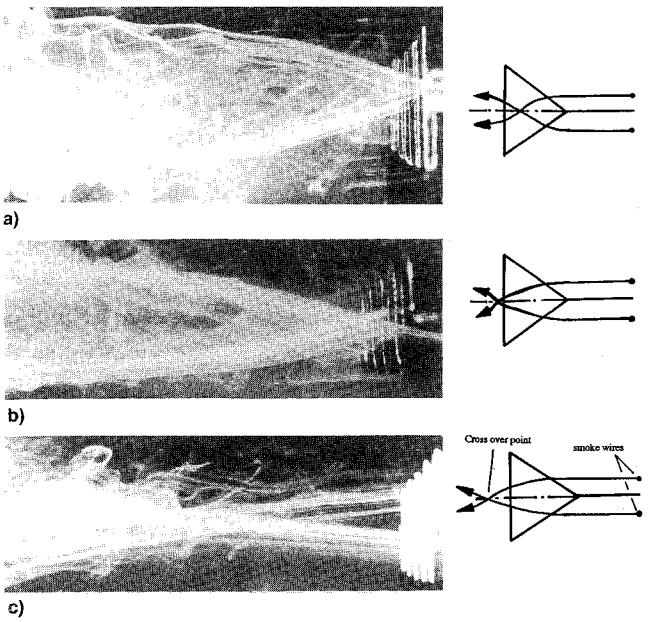

Fig. 3 Visualization of the wake region behind respective lobed mixers: a) square, b) semicircular, and c) triangular (saw-tooth).

Results and Discussion

Initial Conditions

The turbulent boundary-layer thickness of the velocity profiles on either side of the lobed mixer measured at three wavelengths upstream of the penetration region for the three cases were approximately one-third of the wavelength of the lobe. The calculated boundary-layer parameters for the velocity ratio 1:2 are shown in Table 1. Both boundary-layer parameters and boundary-layer profiles indicated that the boundary layers on either side of the lobed mixer were turbulent ($\delta^*/\Theta > 1.3$). Streamwise turbulence levels (measured by the laser-Doppler anemometer) outside the boundary-layer region have maximum values of 2% (normalized by the mean velocity of the local stream) on either side of the lobed mixer at different flow conditions. Further details of the initial conditions can be found in Ref. 12.

Flow Visualization Results

Figures 3a–3c illustrate the photographs of the wake region behind respective mixers for the velocity ratio of 1:1. The location of the crossover point of the top and bottom smokelines near the trailing edge of respective lobed mixers provided some indication on the strength of the secondary flow shed by a particular lobe. The crossover point that appeared within the lobe penetration for the square-lobed mixer suggested strong transverse velocities generated within the lobe penetration region (see Fig. 3a). This crossover location was progressively shifted away from the trailing edge for the semicircular and triangular-lobed mixers (see Figs. 3b and 3c). This suggested a decrease in the magnitude of the transverse velocities. As it will be shown later, the present observation is found to be in qualitative agreement with the measurements. Figures 4a and 4b illustrate the streamwise vortex structure of the semicircular-lobed mixer at the velocity ratio of 1:1. The visualization is achieved by illuminating the flow at a particular streamwise station downstream of the trailing edge using a laser-sheet technique. The formation of the streamwise vortices can be clearly seen in Fig. 4a at $x/\lambda = 4$ downstream of the mixer trailing edge. At this station, two counter-rotating vortices were formed at each lobe and slight asymmetry of the vortex distribution was also observed. By $x/\lambda = 7$ and Fig. 4b downstream, the enlargement of the vortices and mixing by diffusion were obvious. However, no indication of the breakdown of vortices can be found within seven wavelengths downstream of the trailing edge.

Table 1 Boundary-layer parameters at three wavelengths upstream of the penetration region at velocity ratio 1:2

Velocity ratio 1:2	δ^*, mm	Θ, mm	H	Re_Θ
Top stream	1.625	1.166	1.394	1016
Bottom stream	1.437	1.069	1.345	465

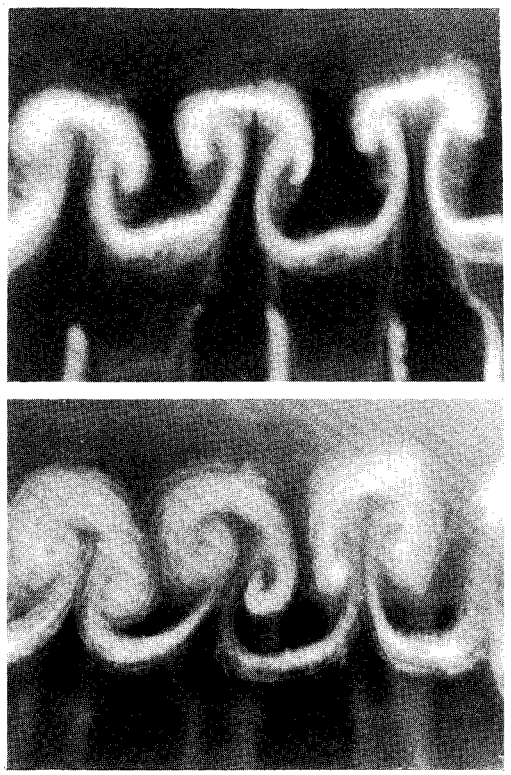

Fig. 4 Visualization of the streamwise vortices at locations downstream of the trailing-edge viewing downstream from the trailing edge (semicircular-lobed mixer). x/λ = a) 4 and b) 7.

Mean Velocities

Velocity Ratio 1:1

Contours of the normalized streamwise mean velocity U/U_r, and the corresponding secondary mean flow vector components ($U_s/U_r = \sqrt{v^2 + w^2}/U_r$, arrow base is at the measuring point), for the square-lobed mixer at $x/\lambda = 0.5$, 2, 4, and 6 are shown in Figs. 5a–5d. The wake region appearing at $x/\lambda = 0.5$ was found to have a larger spread in the square-lobed mixer than the semicircular- and triangular-lobed mixers [see Fig. 5a(ii)]. This may be, in part, due to the boundary-layer growth along the parallel sidewalls and the subsequent shedding of the boundary layer into the wake region. Maximum measured secondary flow velocity at this station for the square-lobed mixer was about 0.45 of the bulk mean velocity, compared to 0.39 for the semicircular lobed mixer and 0.19 for the saw-tooth lobed mixer [see Fig. 5a(i)]. The measurements at this location clearly showed the dominant effects of the parallel sidewalls on the generation of secondary flow. At $x/\lambda = 2$, and in the cases of the square and semicircular lobed mixers, the low momentum fluid shed by the straight ends at $x/\lambda = 0.5$ had been convected to the center region to around $y/\lambda = 0$, $z/\lambda = 0$ as a consequence of the secondary motion created by a lobe [see Figs. 5b(i) and 5b(ii)]. However, in the saw-tooth-lobed mixer, similar observation was not found. This may be partly due to a relatively lower strength of the secondary flow shed by the saw-tooth-lobe geometry. The velocity contours at the wake region for the saw-tooth-lobed mixer only showed diffusion within the projected area of the straight ends. The secondary motion in the square- and semicircular-lobed mixers continued to convect the surrounding

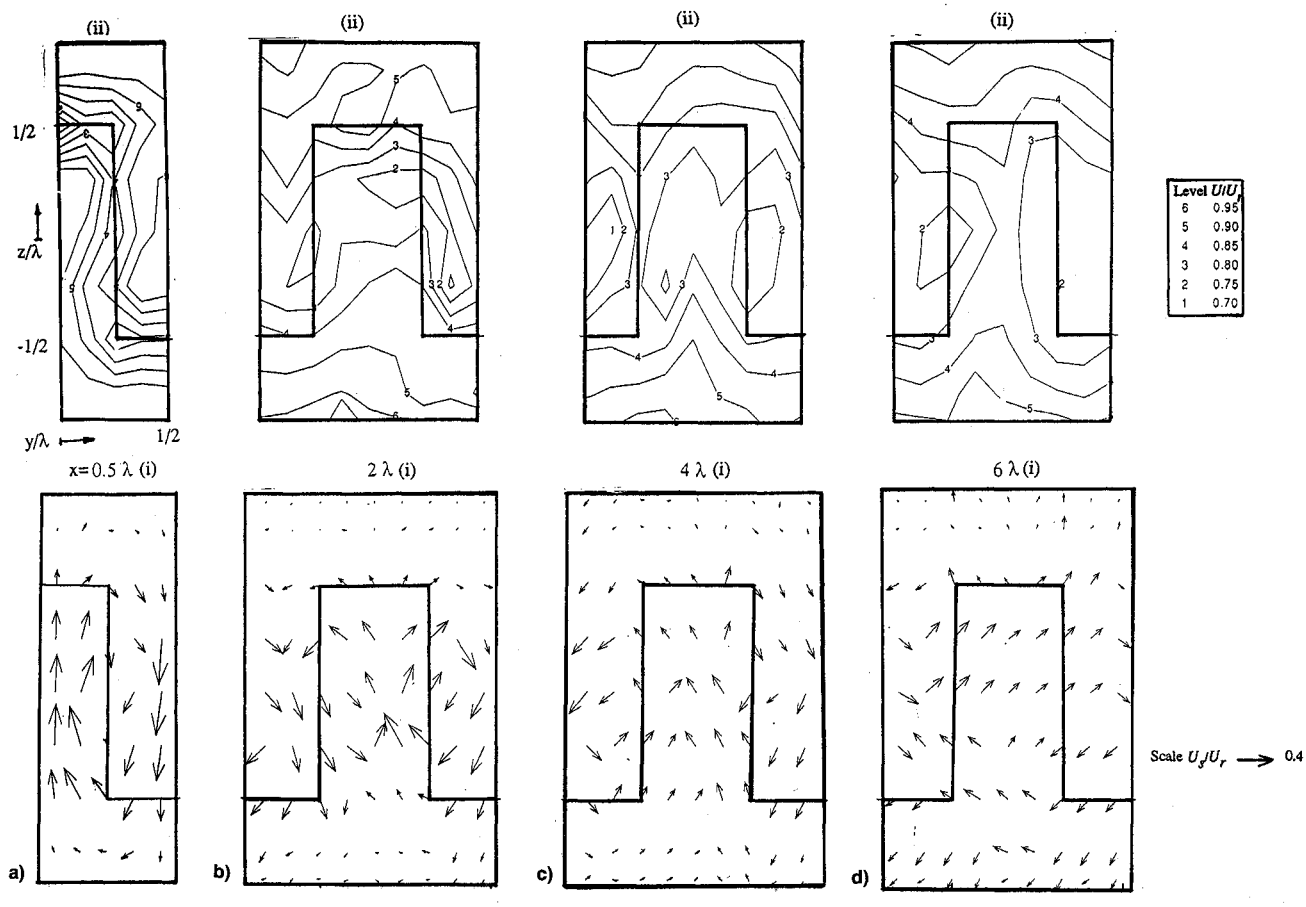

Fig. 5 Contours of the normalized streamwise mean velocity U/U_r and secondary mean velocity vectors U_s/U_r at successive stations downstream of the trailing edge; square-lobed mixer, velocity ratio 1:1.

fluid to the center region, and by $x/\lambda = 4$ and Fig. 5c(ii), some high momentum fluid was also seen to have convected into the center region; this was signified by the bulging of the velocity contours towards the center region at around $y/\lambda = 0$, $z/\lambda = -0.5$. The strength of the secondary flow velocity at this station for the three lobed mixers were approximately 40% lower than those at $x/\lambda = 0.5$ [see Fig. 5c(i)]. Mixing between the low- and high-momentum fluids appeared to have taken place from this location onward so that by $x/\lambda = 6.0$ and Figs. 5d(ii), more uniform distribution of the velocity contours at the center region (i.e., $y/\lambda = 0$, $z/\lambda = 0$) was found in the three cases. The strength of the secondary flow for the three cases at this station was almost the same as in $x/\lambda = 4$ [cf. Figs. 5c(i) and 5d(i)].

Velocity Ratio 1:3

Results for the velocity ratio 1:2 are very similar to those of 1:3. Only the results of the latter are presented in detail here. When the velocities of the two streams were different, with the exception of the triangular lobed mixer, the flows behind the trailing edge of the square and semicircular lobed mixers revealed very different trends from those of the velocity ratio 1:1. At $x/\lambda = 0.5$ and Figs. 6a(i), 7a(i), and 8a(i), the secondary flow pattern developed into pairs of contra-rotating vortices at each lobe with centers at the inflexion point of the lobe contour, i.e., at $y/\lambda = 0.25$ and $z/\lambda = 0$. The highest magnitude of the secondary flow again existed in the square-lobed mixer with a maximum at about 0.48 (about 1% higher than that in the 1:1 case) of the bulk mean velocity, compared to 0.45 (about 6% higher than the 1:1 case) for the semicircular mixer and 0.2 (no change from that of the 1:1 case) for the saw-tooth-lobed mixer for both velocity ratio cases. The convection of the low momentum fluid to the center region for the square- and semicircular-lobed mixers was more obvious at station $x/\lambda = 2$ than the 1:1 case [cf. Figs. 5b(ii) and 6b(ii)]. Steep streamwise mean velocity gradients existed along the y/λ and z/λ directions at a region close to the origin, and they were found to be steeper with the velocity ratio 1:3 case due mainly to a larger difference of the velocities between the two streams. Similar observation, however, was not found in the case of the saw-tooth-lobed mixer at this location [see Fig. 8b(ii)]. Slight asymmetric distribution for the streamwise vortices within a lobe was also observed in the square- and semicircular-lobed mixers at this station [see Figs. 6b(i) and 7b(i)]. Mixing between the high- and low-momentum fluids appeared to have taken place after station $x/\lambda = 2$ and by station $x/\lambda = 4$, a fairly uniform distribution of the contours along the y/λ direction was found [see Figs. 6c(ii) and 7c(ii)]. At the same location behind the saw-tooth-lobed mixer, similar to that in the 1:1 case, the distribution of the contours only showed some diffusion effects around the straight ends of the lobe [see Fig. 8c(ii)]. By station $x/\lambda = 6$ and Figs. 6d(ii) and 7d(ii), further uniformity of the streamwise mean velocity contours along the y/λ direction was achieved in the square- and semicircular-lobed mixers. At the two locations of $x/\lambda = 4$ and 6, the maximum magnitude of the secondary flow velocity was about 0.2 of the bulk mean velocity for the square-lobed mixer, 0.18 for the semicircular-lobed mixer and 0.15 for the saw-tooth-lobed mixer [see Figs. 6c(i), 6d(i), 7c(i), 7d(i), 8c(i), and 8d(i)]. The decay rate of the secondary flow velocity from the trailing edge appeared to be faster for the square- and the semicircular-lobed mixers than the saw-tooth-lobed mixer.

Variation of the Momentum Shape Factor

The mixing of the two flows within the wake region in terms of momentum distribution is of interest. Therefore, it may be sufficient to define mixedness parameter for the two streams in terms of the shape factor of the streamwise mean velocity distribution, i.e.,

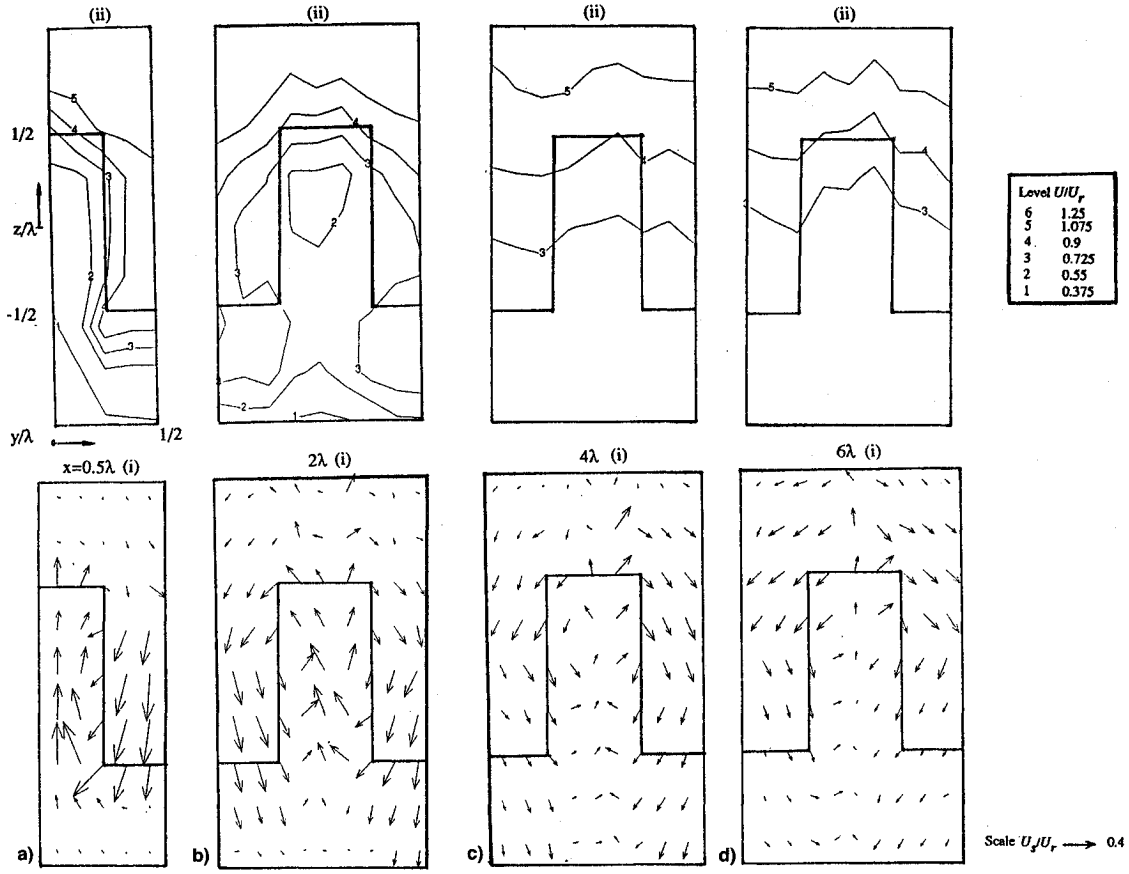

Fig. 6 Contours of the normalized streamwise mean velocity U/U_r and secondary mean velocity vectors U_s/U_r at successive stations downstream of the trailing edge; square-lobed mixer, velocity ratio 1:3.

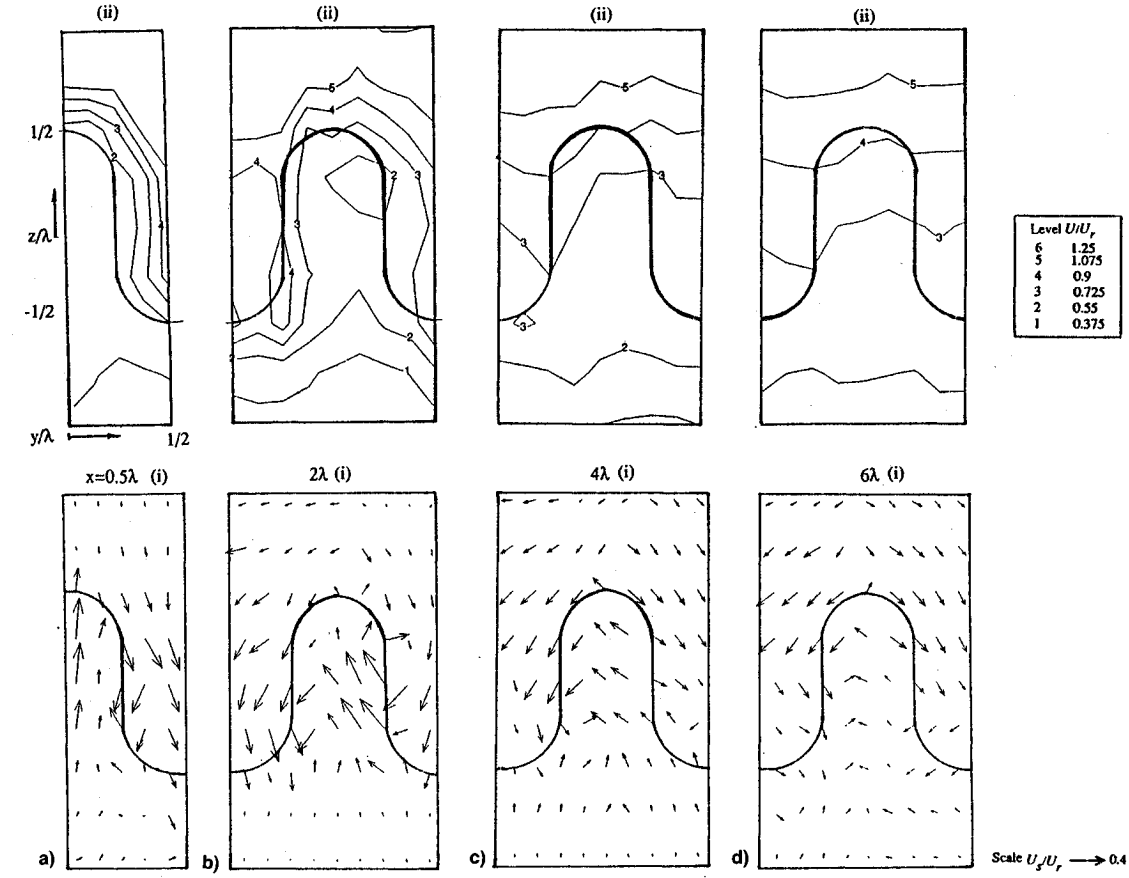

Fig. 7 Contours of the normalized streamwise mean velocity U/U_r and secondary mean velocity vectors U_s/U_r at successive stations downstream of the trailing edge; semicircular-lobed mixer, velocity ratio 1:3.

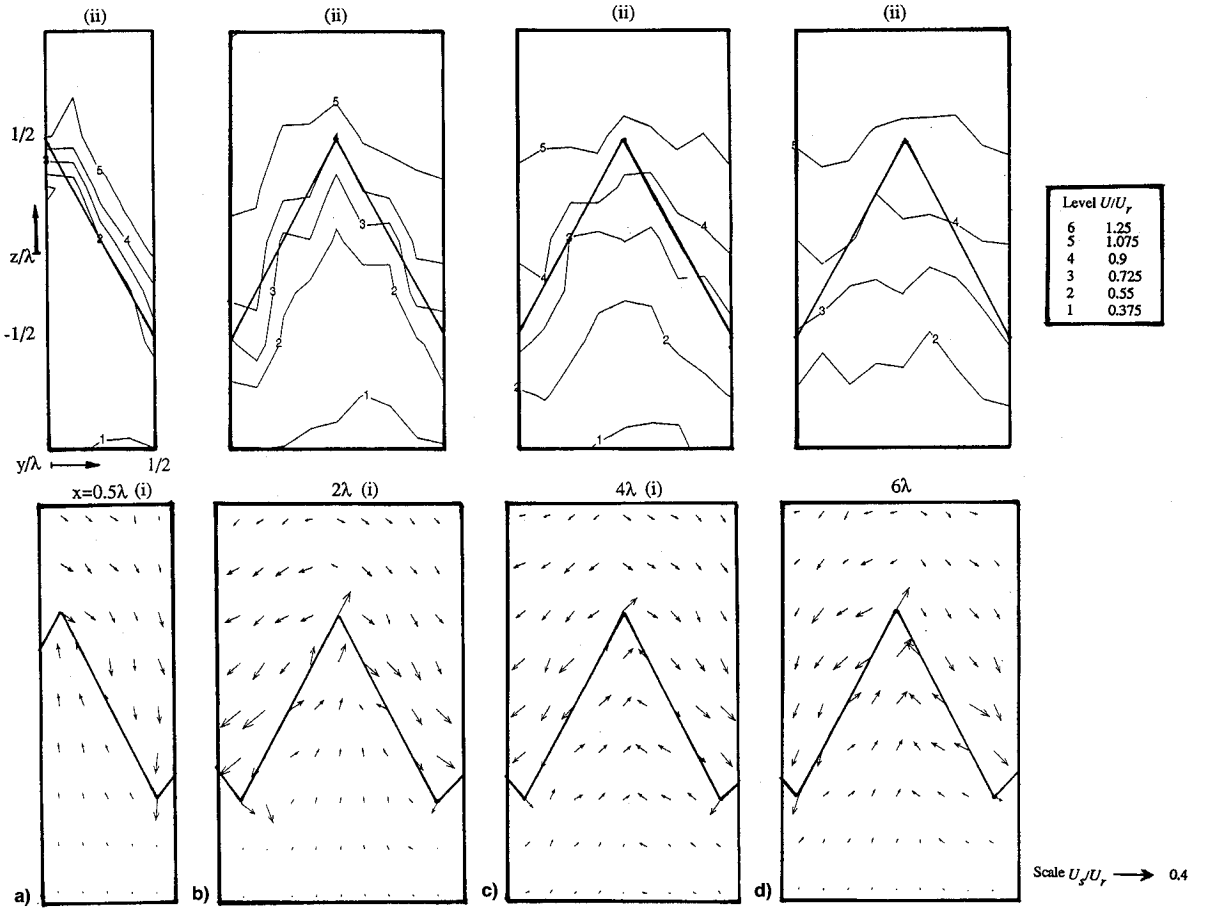

Fig. 8 Contours of the normalized streamwise mean velocity U/U_r and secondary mean velocity vectors U_s/U_r at successive stations downstream of the trailing edge; triangular-lobed mixer, velocity ratio 1:3.

$$S = \left(\int \frac{U^2 \, dA_{\text{wake}}}{U_r^2 A_{\text{wake}}} \right) \tag{1}$$

The definition used here is similar to that used by Bevilaqua[13] to evaluate the thrust distribution due to ejector. Ideally, at the location where the two streams at the wake region with different velocities are to be completely mixed, and spatial uniformity is achieved, the momentum distribution would be uniform and the shape factor should be equal to unity, as illustrated in Fig. 2c. The variation of the shape factor as a function of downstream distance should provide a useful indication of the extent of the spatial uniformity that the two flows can achieve. The wake area boundary is defined by the region bounded by $0 \leq y/\lambda \leq 0.5$ and $U/U_r \leq 0.95$ for the 1:1 case. For the cases of higher velocity ratio, it is defined by the region bounded by $0 \leq y/\lambda \leq 0.5$, and at a location where the influence of the secondary flow to the mean flow is insignificant, i.e., less than 5% of the bulk mean velocity of the two streams.

Variation of the momentum shape factor with the downstream distance for the 1:1 case is very small compared to the 1:2 and 1:3 cases. A maximum deviation of 1% from the ideal mixed condition for the 1:1 case was observed, compared to 12% for the 1:2 case and 22% for the 1:3 case, (cf. Figs. 9a–9c). The calculated results of the shape factor for the 1:1 case were too small to quantify the actual difference between the three configurations since the maximum uncertainty of the shape factor was about 2% (based on the accuracy of the streamwise mean velocity measurements). However, qualitatively, Fig. 9a suggested that the square-lobed mixer that shed the highest secondary flow (streamwise vorticity) had actually created more nonuniformities in the momentum distribution than the semicircular- and triangular-lobed mixers.

For the velocity ratios of 1:2 and 1:3 and Figs. 9b and 9c, the variation of the shape factor for all the lobed mixers showed a decrease in the first one to two wavelengths downstream of the trailing edge, indicating a rapid variation of the momentum distribution within the wake region, as a consequence of streamwise vorticity shed by a lobe. The slopes of the variation curves at this region were also found to be steeper at higher velocity ratios. For the square-lobed mixer, the variation started to level off with the x axis at around $x/\lambda = 3$ and at $x/\lambda = 4$ for the semicircular-lobed mixer in the 1:2 case. These locations appeared to shift closer to the trailing edge as the velocity ratio increased to 1:3, to around $x/\lambda = 2.5$ and $x/\lambda = 3$ for the square- and semicircular-lobed mixers, respectively. At the leveling-off position of the shape factor with the downstream distance, the momentum mixing of the two streams may be considered as completed. The trend for the saw-tooth-lobed mixer showed no signs of leveling off with the x axis within the range of the measurements for both velocity ratios.

In contrast to the 1:1 case, the boundary-layer thickness shed from the lobed mixer sidewalls did not significantly affect the overall mixing performance. The results for the higher velocity ratios clearly showed that the square-lobed mixer that shed the highest strength of the secondary flow among the three lobed mixers can achieve the fastest and highest spatial uniformity than the other two lobed mixer configurations. The increase in the velocity ratio from 1:2 to 1:3 appeared to facilitate this process. Thus, the present measurements agree well with the qualitative tests of Manning.[9]

Variation of the Streamwise Circulation

The strength of the streamwise vorticity at downstream locations may be quantified by evaluation of the streamwise

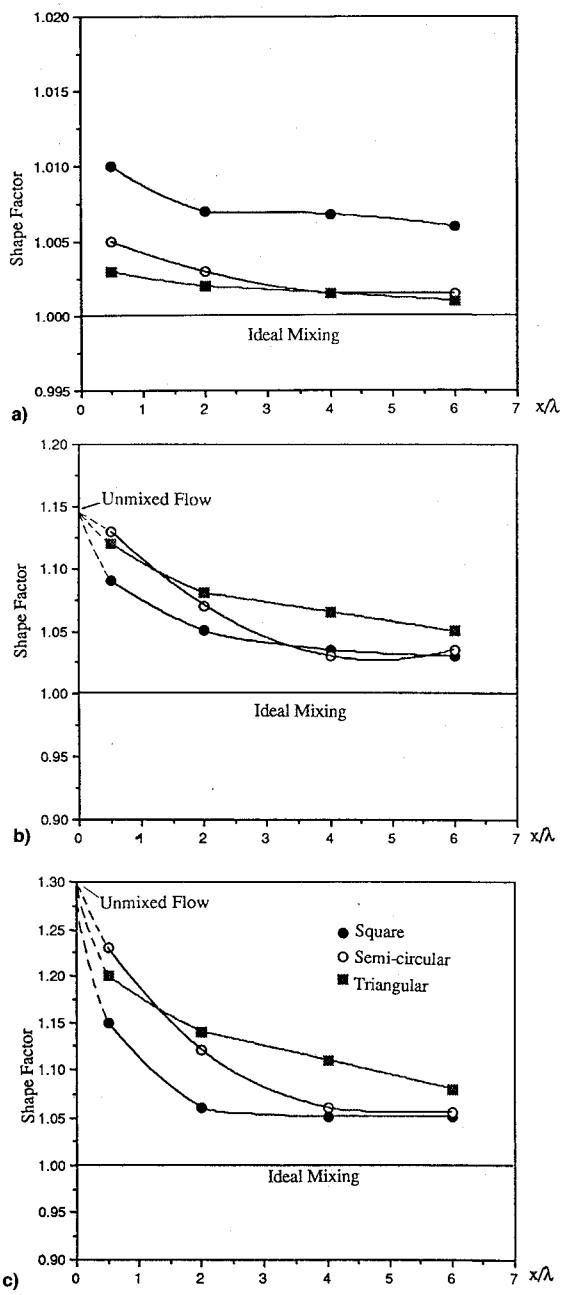

Fig. 9 Variation of shape factor with downstream distance from the trailing edge at velocity ratios of a) 1:1, b) 1:2, and c) 1:3.

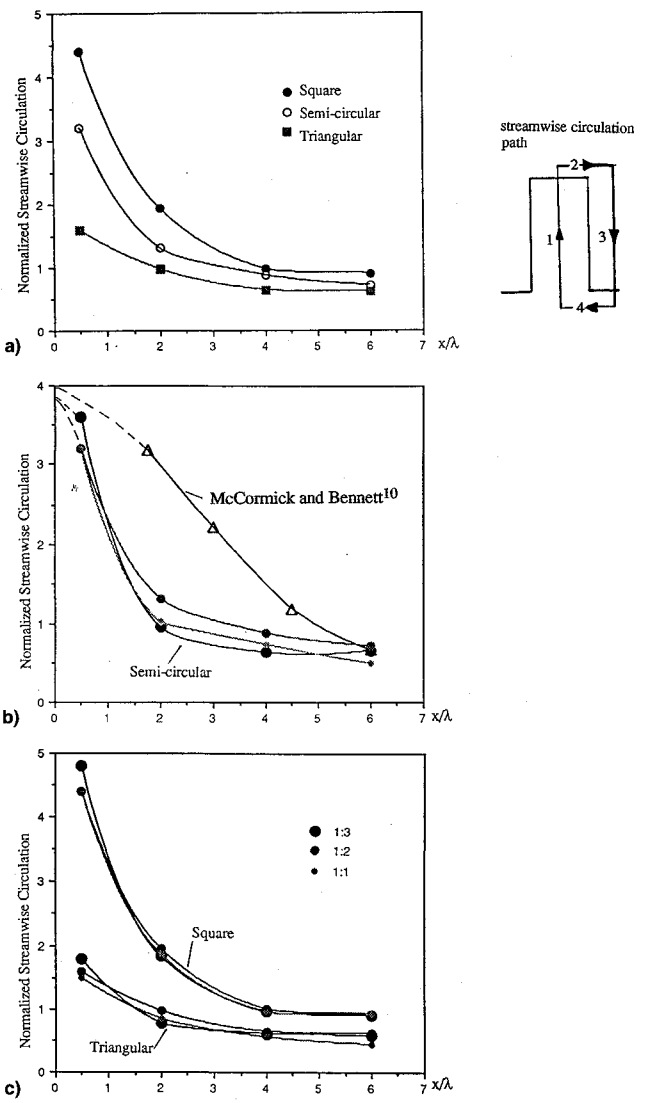

Fig. 10 Variation of streamwise circulation with downstream distance from the trailing edge a) at a velocity ratio of 1:2, b) semicircular-lobed mixer at three velocity ratios, and c) square- and triangular-lobed mixers at three velocity ratios.

circulation along a rectangular path that encompasses one-half the lobe wavelength as shown in Fig. 10. In nondimensional expression

$$C_1 = \frac{\Gamma_s}{U_r h \tan \varepsilon} \tag{2}$$

where

$$\Gamma_s = \oint_{1-2} W\,ds + \oint_{2-3} V\,ds + \oint_{3-4} W\,ds + \oint_{4-1} V\,ds$$

The initial values at the mixer trailing edge (at $x/\lambda = 0.0$) for different cases may be determined using the one-dimensional analysis of Barber et al.[6] Figure 10a shows the variation of the streamwise circulation for respective lobed mixers at a velocity ratio of 1:2 with downstream distance. Computed values near the trailing edge were found to be largest for the square-lobed mixer followed by the semicircular- and the triangular-lobed mixers, as may be expected from lobed mixers consisting of straight parallel sidewalls. The decay rate was also found to be faster in mixers consisted of straight parallel sidewalls within the first four wavelengths; downstream of which, magnitude of the streamwise circulation for the three mixers were almost the same. Similar trends of variation can also be found in the velocity ratio of the 1:3 case.

Figures 10b and 10c show the comparison for respective mixers at different velocity ratios. In the three different velocity ratios (including the 1:1 ratio) and for a particular lobe configuration, similar magnitude and trends of variation for the streamwise circulation with downstream distance were found. This observation suggested that for a particular lobed mixer, the strength of the streamwise vorticity shed by a lobe was not strongly dependent on initial flow conditions, but more on the geometrical conditions. Results for the semicircular-lobed mixer measured by McCormick and Bennett[10] (within the range of $x/\lambda = 0.0$ to 6) were also plotted in Fig. 10b for comparison. The variation of the streamwise vorticity appeared to be more gradual in the case of McCormick et al., although the initial values for both mixers were very similar. This may be due to the formation of the horseshoe vortices as a consequence of higher aspect ratio lobe ($h/B = 3$) used by McCormick et al. However, by $x/\lambda = 6$, the magnitude of the streamwise circulation was nearly the same for both cases.

Turbulence

Due to limited space, only the variation of turbulent kinetic energy at the wake region with distance downstream are presented here, i.e.,

$$f\left(\frac{x}{\lambda}\right) = \int \frac{k\ \mathrm{d}A_{\mathrm{wake}}}{A_{\mathrm{wake}}} \tag{3}$$

The wake area boundaries used for the calculation of the turbulent kinetic energy are the same as those for the calculation of streamwise momentum shape factor.

For the 1:1 case and Fig. 11a, it appeared that the high-turbulence region followed by the vortex breakdown[7] was not present within the measurement range (six wavelengths downstream). However, the trends of decaying in magnitude and the trace of homogeneous turbulence at downstream locations were evident, particularly in the cases of the semicircular and saw-tooth-lobed mixers. For the square-lobed mixer, the variation of the turbulent kinetic energy showed an initial drop in the first two and half wavelengths, and was followed by a gradual rise over a distance of three and a half wavelengths. The reason for this rise, at present, is not very clear, but it may be due to the positive production of turbulent kinetic energy as found in the other two velocity ratios (as will be explained later). However, the increasing rate was not as rapid as in the other two velocity ratios.

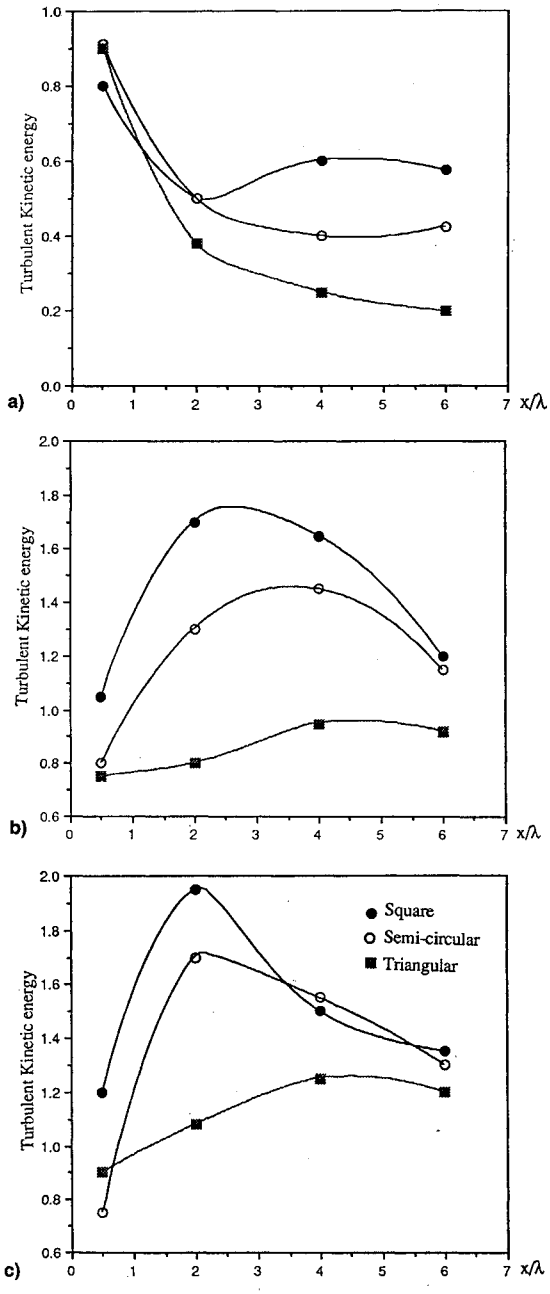

Fig. 11 Variation of wake area average turbulent kinetic energy with downstream distance from the trailing edge at velocity ratios of a) 1:1, b) 1:2, and c) 1:3.

For the cases of higher velocity ratios and Figs. 11b and 11c, an initial increasing trend was shown by all cases, including the saw-tooth-lobed mixer. A distinct peak appeared at around $x/\lambda = 2.5$ and 3.5 for the square- and semicircular-lobed mixers for the velocity ratio 1:2. The peak appeared to shift closer to the trailing edge of the mixers as the velocity ratios increased to 1:3, and were at around $x/\lambda = 2$ and 2.5 for the square- and semicircular-lobed mixers, respectively (cf. Figs. 11b and 11c). The reason for this increase may be explained by analyzing the production terms in the Reynolds stresses equations in relation to the velocity measurements obtained at the corresponding locations.

The production terms for the normal stresses in the Reynolds stresses equations may be written as (in a rectangular Cartesian coordinate system, see Ref. 14, p. 28):

$$G(u'^2) = -2\left(\overline{u'w'}\frac{\partial U}{\partial z} + \overline{u'v'}\frac{\partial U}{\partial y} + u'^2\frac{\partial U}{\partial x}\right) \tag{4}$$

$$G(v'^2) = -2\left(\overline{v'w'}\frac{\partial V}{\partial z} + v'^2\frac{\partial V}{\partial y} + \overline{u'v'}\frac{\partial V}{\partial x}\right) \tag{5}$$

$$G(w'^2) = -2\left(w'^2\frac{\partial W}{\partial z} + \overline{v'w'}\frac{\partial W}{\partial y} + \overline{u'w'}\frac{\partial W}{\partial x}\right) \tag{6}$$

Figures 12a and 12b show the contours of the shear stresses measured at location $x/\lambda = 2$ downstream for the semicircular-lobed mixer at a velocity ratio of 1:2 and square-lobed-mixer at a velocity ratio of 1:3. The sudden surge of the turbulent kinetic energy appeared at the location where the convection of the low momentum fluid to the center region had taken place, i.e., at around $y/\lambda = 0$, $z/\lambda = 0$, and $x/\lambda = 2$. Because of the initial velocity difference and the subsequent secondary convection process, steep streamwise mean velocity gradients were found along the y/λ and z/λ directions [e.g., Figs. 6b(ii) and 7b(ii)]. By considering the signs of the velocity gradients along these two directions in relation to the coordinate system adopted (the signs are positive along both the y/λ and z/λ directions), and the sign of the shear stresses ($\overline{u'v'}$, $\overline{u'w'}$; the signs are negative) measured around this region, the shear stresses and the velocity gradients, in fact had the opposite signs. Thus, they represented a positive contribution in the first two terms for the u'^2 components [Eq. (4)]. However, for the third term in Eq. (5) and the third term in Eq. (6), they suggested a negative contribution for the v'^2 and w'^2 components, respectively. The gradients of $(\partial V/\partial x)$ and $(\partial W/\partial x)$ were negative due to the rapid variation (decay) of streamwise circulation at this region, as shown in Fig. 10a.

At this station, it may be reasonable to assume that the gradients $(\partial U/\partial x)$, $(\partial V/\partial y)$, and $(\partial W/\partial z)$ were small. Then, the effects of the third term in Eq. (4), the second term in Eq. (5), and the first term in Eq. (6) may become insignificant to the overall contribution. Since the shear stress $\overline{v'w'}$ components were not measured, the influence of which in the first term in Eq. (5) and the second term in Eq. (6) cannot be determined. However, the overall trend was still a positive gain in the turbulent kinetic energy, as shown in Figs. 11b and 11c and for individual stresses components.[12]

It is also interesting to note that the locations of the peak in the variation of turbulent kinetic energy with downstream distance are very close to the locations where the strength of the streamwise circulation and the spatial uniformity of the momentum (shape factor) have almost reached a steady level (cf. Figs. 9c, 10c, and 11c).

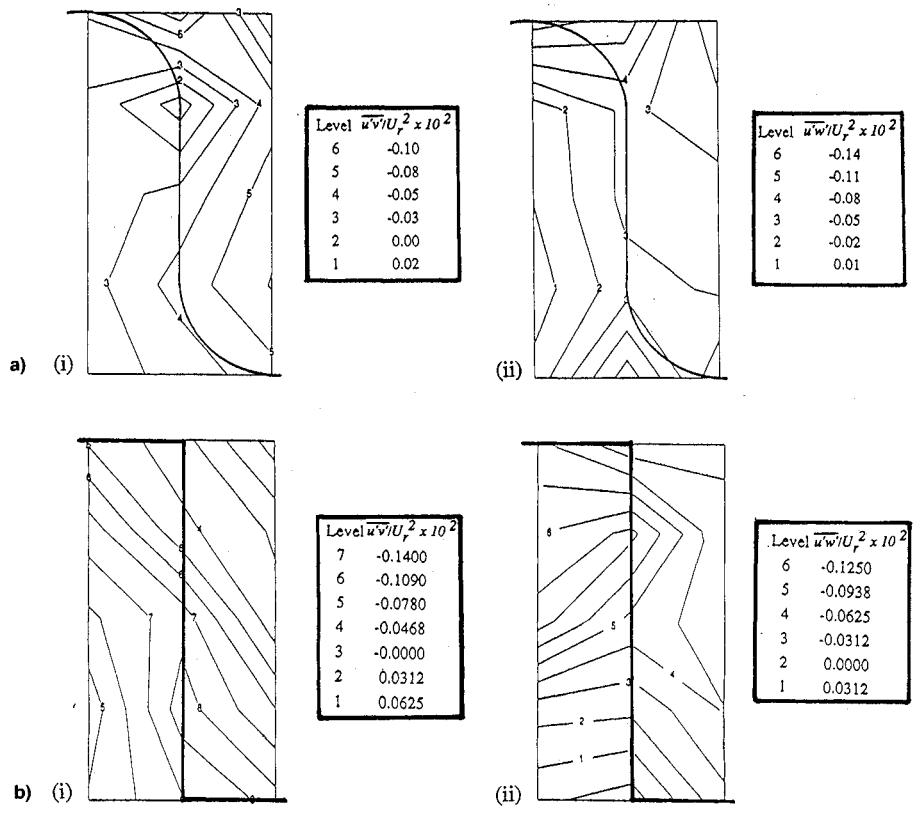

Fig. 12 Contours of normalized shear stresses ($\overline{u'v'}/U_r^2$, $\overline{u'w'}/U_r^2$) at station $x/\lambda = 2$ downstream of the trailing edge: a) semicircular and b) square-lobed mixers.

Summary

For a 1:1 velocity ratio, the measurements for the three different configurations of a lobed-forced mixer indicated that the strength of the secondary flow shed by the lobe was higher with lobed mixers consisting of straight parallel sidewalls. The boundary-layer thickness, generated along the sidewalls of the lobe and the subsequent shedding of the boundary layer into the wake region, was also found to be an important factor in affecting the uniformity of the momentum distribution. High-turbulence regions were not detected within the six wavelengths downstream of all the lobed mixers investigated. The turbulence measurements had actually shown trends of decay in magnitude and became more homogeneous at downstream locations.

For the velocity ratios of 1:2 and 1:3 and in contrast to those in the 1:1 case, the boundary-layer thickness shed from the lobed mixer sidewalls had not significantly affected the overall mixing performance. The measurements for the three different configurations of a lobed-forced mixer indicated that the higher strength of the streamwise vorticity shed by a lobe would result in a faster rate of achieving spatial uniformity at a downstream distance. However, the strength of the streamwise vorticity shed by a particular lobe configuration did not increase significantly with higher velocity ratios. This suggested that for a particular lobed mixer, the strength of the streamwise vorticity shed by a lobe was not strongly dependent on initial flow conditions but was more dependent on the geometrical conditions. A peak in the variation of turbulent kinetic energy with downstream distance appeared at around $x/\lambda = 2.5$ and 3.5 for the square- and semicircular-lobed mixers for the velocity ratio 1:2. The peaks appeared to shift closer to the trailing edge of the mixers as the velocity ratio increased to 1:3, and were at around $x/\lambda = 2$ and 2.5 for the square- and semicircular-lobed mixers, respectively. No distinct peak was found in the triangular-lobed mixer case. Analyzing the production terms in the Reynolds stresses equations at the location corresponded to two wavelengths downstream of the square- and semicircular-lobed mixers suggested that positive production of turbulent kinetic energy existed and was a consequence of large mean axial flow shear gradients coinciding with shear stresses of the opposite signs. The large mean axial flow shear gradients were created first by the velocity difference between the two streams, and were enhanced subsequently by the generation of the secondary flows by the lobe. Thus, the present measurements suggested that the high turbulence that would be responsible for rapid mixing may be a result of the positive production of turbulent kinetic energy at locations about two to three wavelengths downstream of the trailing edge, rather than due to the mechanism of vortex breakdown.

Acknowledgments

Financial support for this project from the NTU Applied Research Grant, and a Research Assistantship for J. K. L. Teh from the School of Mechanical and Production Engineering, Singapore, are gratefully acknowledged.

References

[1]Presz, W. M., Blinn, R. F., and Morin, B., "Short Efficient Ejector Systems," AIAA Paper 87-1837, Jan. 1987.

[2]Presz, W. M., Gousy, R., and Morin, B., "Forced Mixer Lobes in Ejector Design," *Journal of Propulsion and Power*, Vol. 4, No. 4, 1988, pp. 350–355.

[3]Malecki, R., Mityas, S., and Lord, W., "Navier-Stokes Analysis of an Ejector and Mixer Ejector Operating at Pressure Ratio in the Range 2-4," AIAA Paper 90-2730, July 1990.

[4]Paterson, R. W., "Turbofan Forced-Mixer Nozzle Internal Flow Field Vol. 1: A Benchmark Experimental Study," NASA CR3492, April 1982.

[5]Paterson, R. W., "Turbofan Mixer Nozzle Flowfield—A Benchmark Experimental Study," *Journal of Engineering for Gas Turbines and Powers*, Vol. 106, July 1984, pp. 692–698.

[6]Barber, T., Paterson, R. W., and Skebe, S. A., "Turbofan Forced Mixer Lobe Flow Modeling Vol. 1: Experimental and Analytical Assessment," NASA CR4147, 1988.

[7]Werle, M. J., Paterson, R. W., and Presz, W. M., Jr., "Flow Structure in a Periodic Axial Vortex Array," AIAA Paper 87-0610, Jan. 1987.

[8]Eckerle, W. A., Sheibani, H., and Awad, J., "Experimental Measurement of the Vortex Development Downstream of a Lobed Forced Mixer," *Journal of Engineering for Gas Turbines and Power*, Vol. 114, Jan. 1992, pp. 63–71.

[9]Manning, T. A., "Experimental Studies of Mixing Flows with Streamwise Vorticity," M.S. Thesis, Massachusetts Inst. of Technology, Cambridge, MA, Sept. 1991.

[10]McCormick, D. C., and Bennett, J. C., Jr., "Vortical and Turbulent Structure of a Lobed Forced Mixer Free-Shear Layer," AIAA Paper 93-0219, Jan. 1993.

[11]Yu, S. C. M., Yeo, J. H., and Teh, J. K. L., "Some Measurements Downstream of a Lobed Forced Mixer with Different Trailing Edge Configurations," *International Communications in Heat and Mass Transfer*, Vol. 20, No. 5, 1993, pp. 721–728.

[12]Teh, J. K. L., "Flow Field Characteristics of a Forced Lobed Mixer with Different Trailing Edge Configurations at Different Velocity Ratios," M.S. Thesis, Nanyang Technological Univ., Singapore, April 1994.

[13]Bevilaqua, P. M., "Evaluation of Hypermixing for Thrust Augmentation Ejector," *Journal of Aircraft*, Vol. 11, No. 6, 1974, pp. 348–354.

[14]Bradshaw, P., Cebeci, T., and Whitelaw, J. H., *Engineering Calculation Methods for Turbulent Flow*, Academic Press, 1981, p. 28.